Energy flow in piezoelectric energy harvesting systems

Junrui Liang and Wei-Hsin Liao[1]

Smart Materials and Structures Laboratory, Department of Mechanical and Automation
Engineering, The Chinese University of Hong Kong, Shatin, N T, Hong Kong,
People's Republic of China

E-mail: whliao@cuhk.edu.hk

Abstract
In the research of piezoelectric energy harvesting (PEH), the previous foci were mostly on the
amount of energy that can be harvested from the ambient vibration sources. Other portions of
energy, e.g., the energy dissipated during the harvesting process, were seldom considered in
PEH systems. Yet, the ignorance on these energies might cause some misunderstanding in the
studies of energy harvesting. This paper sets up an energy flow based framework for the analysis
of PEH systems. An energy flow chart is introduced to comprehensively illustrate the energy
paths within the PEH system. Taking the interface circuits of standard energy harvesting (SEH)
and synchronized switch harvesting on inductor (SSHI) as examples, different branches of
energy flow in the PEH systems are quantitatively investigated. In the previous literature, only
the harvested energy was emphasized as a function of the rectified voltage or its corresponding
DC load resistance. To be more general, we show that both the harvesting energy and dissipated
energy change with the rectified voltage; in addition, these two portions of energy also depend
on the ratio between the rectifier voltage drop and the open circuit voltage. Three experiments
are carried out with an SSHI device to measure its performances on energy harvesting, energy
dissipation, and structural damping. The experimental results show good agreement with
theoretical analysis. The functional relations among these branches of energy flow are found.

(Some figures in this article are in colour only in the electronic version)

1. Introduction

A wireless sensor network (WSN) consists of different kinds of
spatially distributed autonomous sensors to monitor the health
of military and civil infrastructures [1]. Unlike traditional
sensor systems, the power supply for the wireless sensor
networks (WSNs) is an issue. Yet, nowadays, most of the
sensing and transmitting units used in WSNs are still powered
by batteries. The use of batteries in these devices restricts
both their lifetime and installation in places where batteries are
hard to replace. Such a problem could be hopefully overcome
with the development of the techniques of energy harvesting
(also known as power harvesting and energy scavenging).
With these techniques, ambient energy in certain forms can
be converted, and stored in electrical form, so as to power the

---

[1] Author to whom any correspondence should be addressed.

wireless electronics. For example, with its electromechanical
coupling characteristic, piezoelectric material can be utilized
to scavenge the mechanical energy associated with ambient
vibration.

Most of the recent researches on piezoelectric energy
harvesting (PEH) have been focused on improving the
efficiency of PEH devices with respect to three main
considerations, i.e., mechanical configuration, interface circuit
and energy storage [2]. The studies emphasizing the
mechanical part usually simply regarded the harvesting
interface circuit as being equivalent to a linear resistive
load [3–6]; therefore, the details of energy flow within the
real interface circuits were overlooked in these studies. On
the other hand, in a majority of studies emphasizing the
electrical part, the branches of energy flow other than the
harvesting one also received little attention [7–11]. In some
cases, the harvested energy and extracted energy were even

confused [12, 13]. Neglecting other branches of energy flow might cause the misunderstanding of some detailed insights in the PEH system.

The analysis on different branches of energy flow is crucial towards the overall evaluation of the performances of PEH devices, as well as the clarification on the design target for these devices. Energy flow charts were presented in [14, 15] to illustrate the energy flow within the PEH devices; yet, no further analysis on different branches of energy flow was provided in these literatures. Detailed analysis should quantitatively take different branches into consideration. Lesieutre *et al* [16] studied the structural damping effect (related to energy extraction) induced by energy harvesting in the standard energy harvesting (SEH) device. Liang and Liao [17] later pointed out that, in the synchronized switch harvesting on inductor (SSHI) device, two functions of energy harvesting and energy dissipation are coexistent, and both of them bring out structural damping. Guyomar *et al* [18] studied the difference between the extracted energy and harvested energy in SSHI devices, and found that the harvested energy is not a linear function of the extracted energy.

This paper is aimed at setting up an energy flow based framework for the analysis of PEH systems. The functional relations among the harvested energy, dissipated energy, extracted energy, and vibratory energy in the PEH system are clarified throughout the paper. These four branches of energy flow are inevitably coexistent within the harvesting process. Section 2 introduces the principle of the PEH device. Section 3 gives an overview of the energy flow within the device. Taking SEH and SSHI devices as examples, section 4 provides a quantitative analysis on different branches of energy flow. Section 5 introduces the experiments that are carried out to measure the three evaluating factors for the PEH systems. Section 6 gives the conclusion.

2. PEH device

Piezoelectric, electromagnetic, and electrostatic transduction mechanisms are three types of commonly investigated mechanisms that can be utilized to harvest energy from ambient vibration. In terms of mechanical configuration, the PEH devices are the simplest type among the three [19]. Figure 1 shows the configuration of a cantilevered PEH device. A piezoelectric patch is bonded to the cantilever surface, which is under alternating deformation. The poling direction of the piezoelectric patch is perpendicular to the structural surface; therefore it is working under 3–1 mode. A circuit is connected to the electrodes of the piezoelectric patch. Generally speaking, various circuits could be designed for different objectives; yet, in terms of energy flow, they all extract energy from the vibrating mechanical structure. For the purpose of vibration control, usually the extracted energy is dissipated; while for energy harvesting, a portion of the extracted energy is reclaimed and stored in electrical form for subsequent usage. As illustrated in figure 1, for a PEH device, the interface circuit provides power conditioning, and
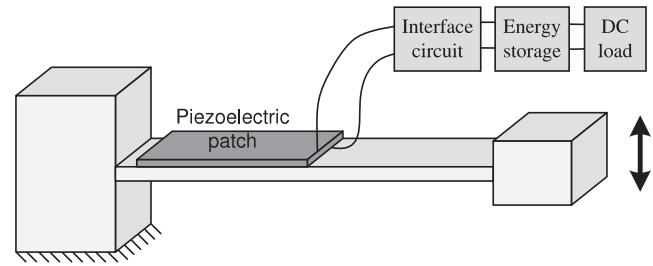

Figure 1. A typical cantilevered PEH device.

the energy storage device stores the harvested energy, while a part of the harvested energy is used to power the DC load.

Figure 2 shows the single degree-of-freedom (SDOF) schematic representation of this PEH device. The mechanical cantilevered structure is modeled as a mass–spring–damper system, whose effective mass, inherent damping, and stiffness are denoted as M, D, and K in the figure, respectively. The details of the coupling mechanism within the piezoelectric element are also illustrated. The piezoelectric element is composed of the piezoelectric short circuit stiffness K_p, an ideal electromechanical transducer with a force–voltage factor of α_e, and the clamped capacitance of the piezoelectric element C_p. $F(t)$ and $x(t)$ are the applied force and displacement of the cantilever; $v_p(t)$ and $i_p(t)$ are the voltage across and current flowing out the piezoelectric element, respectively.

To further analyze the behaviors of the electromechanical device, the coupling mechanism of the piezoelectric element should be equivalently modeled in either a mechanical or electrical representation [20]. With the harvesting interface circuit, the electrical part of a PEH device is nonlinear; its behavior is not easy to model with mechanical equivalence. It is more convenient to convert the mechanical part into electrical equivalence. The dynamics of the SDOF representation shown in figure 2 can be represented by the following equations:

$$F(t) = M\ddot{x}(t) + D\dot{x}(t) + (K + K_p)x(t) + \alpha_e v_p(t)$$
$$i_p(t) = \alpha_e \dot{x}(t) - C_p \dot{v}_p(t). \tag{1}$$

Taking

$$v_{eq}(t) = \frac{F(t)}{\alpha_e}; \qquad i_{eq}(t) = \alpha_e \dot{x}(t); \tag{2}$$

$$L = \frac{M}{\alpha_e^2}; \qquad R = \frac{D}{\alpha_e^2}; \qquad C = \frac{\alpha_e^2}{K + K_p} \tag{3}$$

and rearranging (1), two connection relations in the equivalent circuit can be obtained from (1) as

$$v_{eq}(t) = L\frac{di_{eq}(t)}{dt} + Ri_{eq}(t) + \frac{1}{C}\int_0^t i_{eq}(\iota)\,d\iota + v_p(t) \tag{4}$$
$$i_{eq}(t) = i_p(t) + C_p \dot{v}_p(t).$$

With the voltage relation given by the first equation in (4), the equivalent voltage source v_{eq}, equivalent inductance L, equivalent resistance R, equivalent capacitance C, and v_p are connected in series; while with the current relation given by
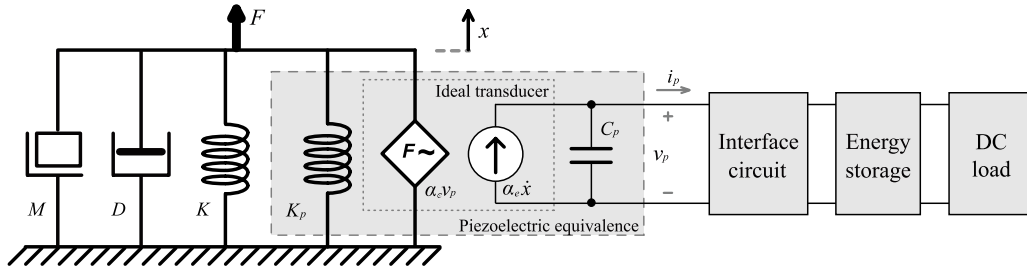
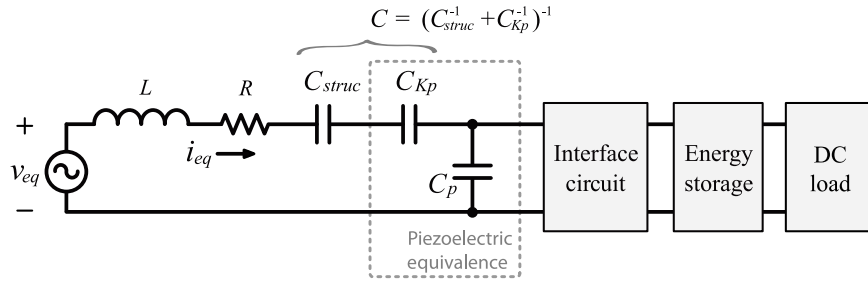**Figure 2.** SDOF schematic representation of a PEH device.

Figure 3. Equivalent circuit of a PEH device.

the second equation, C_{p} and the interface circuit are connected in parallel. Based on these relations, figure 3 illustrates the equivalent circuit of the corresponding PEH device. The values of these parameters in the equivalent circuit can be obtained by an analytical method [21], numerical analysis [22], or experimental identification [23]. In the equivalent circuit, the capacitance C is combined with two capacitances C_{struc} and $C_{K\mathrm{p}}$ in series, which are related to the structural stiffness K and piezoelectric short circuit stiffness K_{p} with the following relations:

$$C_{\mathrm{struc}} = \frac{\alpha_{\mathrm{e}}^2}{K}; \qquad C_{K\mathrm{p}} = \frac{\alpha_{\mathrm{e}}^2}{K_{\mathrm{p}}}. \qquad (5)$$

The device coupling coefficient k_{d}^2 is defined as

$$k_{\mathrm{d}}^2 = \frac{\alpha_{\mathrm{e}}^2}{(K + K_{\mathrm{p}})C_{\mathrm{p}} + \alpha_{\mathrm{e}}^2} = \frac{C}{C + C_{\mathrm{p}}}. \qquad (6)$$

To emphasize the energy flow in the harvesting interface circuits, rather than the dynamics of the overall PEH system, displacement excitation is considered in this paper, i.e., let

$$x(t) = -X\cos(\omega t) \qquad (7)$$

where the displacement magnitude X is constant in the harmonic vibration, and ω is the excitation frequency. Given the relation between $\dot{x}(t)$ and $i_{\mathrm{eq}}(t)$ in (2), the equivalent current is obtained as

$$i_{\mathrm{eq}}(t) = \alpha_{\mathrm{e}}\omega X \sin(\omega t). \qquad (8)$$

When the excitation frequency ω is unchanged, i_{eq} can be regarded as a current source whose magnitude is $I_0 = \alpha_{\mathrm{e}}\omega X$. Therefore, under displacement excitation, the equivalent circuit in figure 3 is further simplified into figure 4. The voltage source v_{eq}, inductance L and resistance R in figure 3
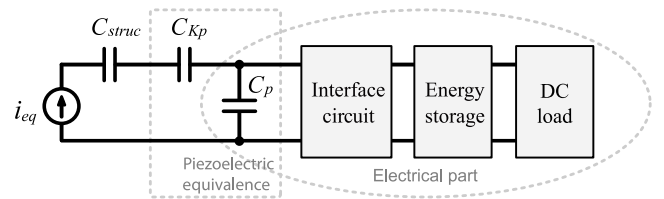

Figure 4. Equivalent circuit under constant displacement excitation.

are substituted by the current source i_{eq} in figure 4. The capacitances C_{struc} and $C_{K\mathrm{p}}$ are kept for the quantitative evaluation of the vibratory energy. Without these two capacitances, the equivalent circuit is the same as those in [7, 11, 24, 25], which was called the uncoupled model by Shu and Lien [26]. Inclusion of the equivalent capacitance C, which corresponds to the short circuit stiffness of the piezoelectric structure, in the equivalent circuit is useful for the evaluation of the structural effect induced by energy harvesting and dissipation.

Based on (8), the charge flowing through the equivalent circuit is given by

$$Q_{\mathrm{eq}}(t) = \int i_{\mathrm{eq}}(t)\,\mathrm{d}t = -\alpha_{\mathrm{e}}X\cos(\omega t). \qquad (9)$$

If there is no circuit connected, i.e., open circuit, $i_{\mathrm{p}}(t) = 0$; all the charge flowing into the electrical part[2] accumulates in C_{p}. Therefore, the open circuit voltage across the piezoelectric element is given by

$$v_{\mathrm{p,oc}}(t) = \frac{1}{C_{\mathrm{p}}}\int i_{\mathrm{eq}}(t)\,\mathrm{d}t = -V_{\mathrm{OC}}\cos(\omega t) \qquad (10)$$

---

[2] The electrical part includes C_{p} and the harvesting circuit, as illustrated in figure 4.
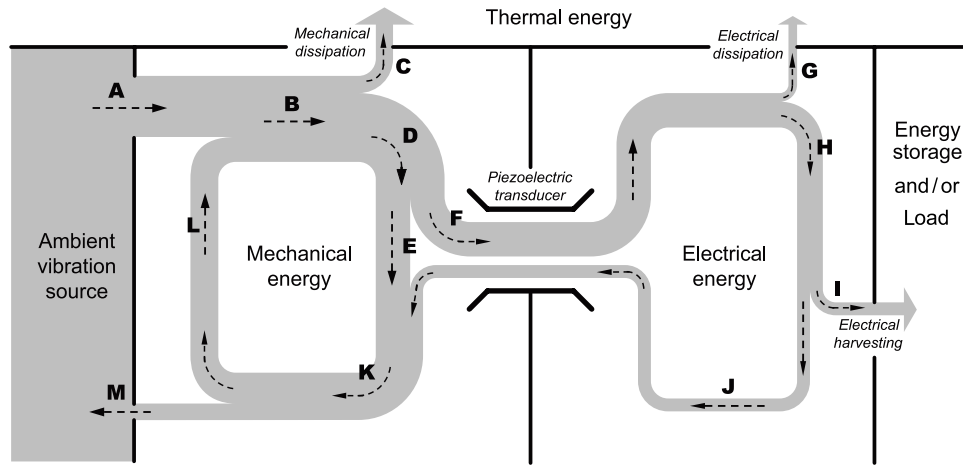
Figure 5. Energy flow chart in general PEH devices.

where

$$V_{\text{OC}} = \frac{I_0}{\omega C_p} = \frac{\alpha_e X}{C_p} \qquad (11)$$

is the magnitude of the open circuit voltage $v_{p,\text{oc}}$.

3. Overview of the energy flow

Most of the literatures, which emphasized the mechanical part in PEH, took a resistor as the AC load to represent the entire harvesting circuit, so as to estimate the harvested power. From the research point of view, it is understandable, in particular when the mechanical model is complicated. However, from the practical point of view, Mitcheson *et al* [27] pointed out that a pure resistive AC load is not useful and a typical load will be a diode rectifier and smoothing capacitor, i.e., SEH interface. Besides, no matter whether resistive equivalence is practical or not, this oversimplification might lead to neglect of some important details in PEH systems, e.g., the effect of some branches of energy flow. Without considering the real harvesting circuit, different energy compositions in the electrical part cannot be specified. Although the harvested energy is the target of PEH, other portions of energy might also influence the dynamics of the harvested system, and conversely have some effect on the harvesting energy. A scrutiny on the energy flow within PEH systems is of importance.

The energy flow chart provides an intuitive way to indicate the directions of different branches of flow in every vibration cycle. During each cycle, the ambient excitation source inputs energy into the system in mechanical form

(branch **A**). A portion of the energy keeps cycling in the mechanical domain as the vibratory energy (loop **B**–**D**–**E**–**K**–**L**–**B**). Accompanied by the vibration, some mechanical energy is dissipated, i.e., converted into thermal energy (branch **C**), while some is converted into electrical energy (branch **F**) with the electromechanical coupling characteristic of the piezoelectric transducer. In the electrical domain, without the circuit connected, i.e., under open circuit condition, the electrical energy is temporarily stored in the piezoelectric capacitance and then all returns to the mechanical part; however, with different interface circuits connected, this electrical energy may have different destinations. Generally, there are three possible ways:

(a) being converted into thermal energy (branch **G**), i.e., dissipated;
(b) being stored in energy storage devices and/or used to power the load (branch **I**), i.e., harvested;
(c) returning to the mechanical domain (branch **J**).

Finally, if the total mechanical impedance of the piezoelectric device does not match the source impedance, some energy will return to the source (branch **M**).

Energy harvesting and energy dissipation are two basic functions that take place inside a PEH device. Due to the non-ideal characteristics of practical electrical components, the interface circuit inevitably produces energy dissipation during the harvesting process. Even in the SEH, the simplest interface circuit, the bridge rectifier consumes power, because of the diodes' non-zero forward voltage drop. Both functions of energy harvesting and dissipation extract energy from the system, and consequently bring out structural damping.

Three terms are defined, in order to provide performance evaluation and comparison among the two functions of energy harvesting, energy dissipation and their effect on structural damping. A harvesting factor is defined to evaluate the harvesting capability as

$$\eta_h = \frac{E_h}{2\pi E_{\text{max}}} \qquad (12)$$

Figure 5 provides an overview of three forms of energy involved in the PEH devices. These three forms are mechanical, electrical, and thermal. The mechanical and electrical forms are linked by the bi-directional piezoelectric transducer. At the same time, either mechanical or electrical energy can be converted into thermal energy by dissipative elements such as mechanical dampers or electrical resistors. Once the energy is dissipated, i.e., transforms into heat, it will not be recovered in the devices, therefore dissipative transformation is uni-directional.

4

where E_h denotes the harvested energy in one cycle (branch **I**), E_{max} is the energy associated with vibration (branch **K**, the total cycling energy), multiplying by 2π to obtain the vibratory energy in one cycle. A dissipation factor is defined to evaluate the dissipation capability as

$$\eta_d = \frac{E_d}{2\pi E_{max}} \qquad (13)$$

where E_d is the dissipated energy in one cycle (branches **C** and **G**). The mechanical dissipation (branch **C**) is related to the structural characteristics, e.g., material, configuration, which are not directly related to the harvesting circuit. Since this paper is focused on the analysis on the relations among different branches of energy flow in the electrical domain, only the electrical dissipation (branch **G**) is included in the following discussion. With (12) and (13), the loss factor is defined as

$$\eta_\Sigma = \frac{\Delta E}{2\pi E_{max}} = \eta_h + \eta_d \qquad (14)$$

where ΔE is the sum of E_h and E_d, which represents the total removed energy from the vibrating structure in one cycle. The loss factor is related to the capability of vibration damping, which is the combined effect of both energy harvesting and dissipation.

4. Energy flow in SEH and SSHI

WSNs and portable electronics are the best potential applications for PEH techniques [28]. DC power supply is required in these electronic devices. On the other hand, the storage of electrical energy also requires electrical energy in DC form. The interface circuit in the PEH device is mainly used to fulfill the AC–DC conversion.

The SEH is the simplest and widest used harvesting interface circuit. It is fully passive, i.e., does not need any control; therefore, it is easier to implement and more reliable than other non-passive interface circuits. Figure 6(a) shows the circuit topology of the SEH interface. It is composed of a bridge rectifier for AC rectification, a filter capacitor, C_{rect}, for filtering and energy storage, and a DC load, R_{load}. Given the harmonic current i_{eq} in (8), figure 6(b) shows the typical waveforms of i_{eq}, v_p, and their product, i.e., the power entering the electrical part. The voltage across the piezoelectric element in SEH can be described by the piecewise equation

$v_{p,SEH}(t)$

$$= \begin{cases} v_{p,oc}(t) - v_{p,oc}(0) - V_{rect}, & 0 \leqslant \omega t < \theta \\ V_{rect}, & \theta \leqslant \omega t < \pi \\ v_{p,oc}(t) - v_{p,oc}(\pi/\omega) + V_{rect}, & \pi \leqslant \omega t < \pi + \theta \\ -V_{rect}, & \pi + \theta \leqslant \omega t < 2\pi \end{cases}$$
$$(15)$$

where V_{rect} is the rectified voltage, i.e., the sum of V_{store} (the voltage across C_{rect}) and V_F (the forward voltage drop of the bridge rectifier); θ corresponds to the rectifier blocked interval in a half cycle, as illustrated in figure 6(b). Because C_{rect} is usually selected to be much larger than C_p, v_p is regarded


(a)

(b)
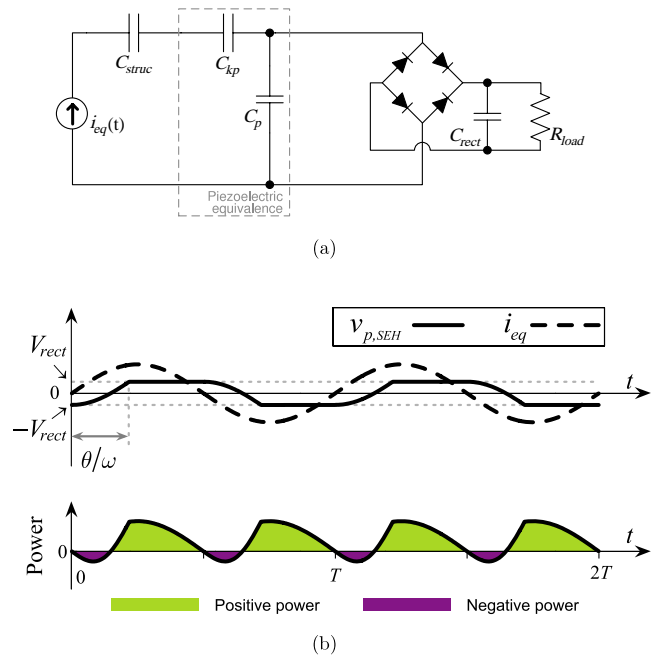
Figure 6. The SEH interface circuit. (a) Circuit topology. (b) Typical waveforms.

constant when the bridge rectifier conducts, e.g., within the $[\theta, \pi)$ or $[\pi + \theta, 2\pi)$ intervals.

Besides performing AC–DC conversion, as an ingredient in the electrical part, the behavior of the interface circuit also influences the energy flow as well as the dynamics of the PEH device. The technique of SEH provides a simple and reliable solution for harvesting ambient vibration energy; however, its harvesting capability is difficult to further enhance. From the power waveform shown in figure 6(b), in most of a cycle, the power is positive, which means that energy is converted from mechanical to electrical; but in some intervals, it has negative value, which indicates that the energy returns from the electrical part to the mechanical part. We call this the energy return phenomenon.

In order to improve the energy conversion efficiency, Guyomar *et al* proposed the SSHI technique [18, 29]. The principle of synchronized switching is similar to that of vibration control with state-switched piezoelectric materials [30, 31]. The SSHI interface circuit reverses the voltage across the piezoelectric element at the transition instants from short to open circuit [32]. Shu *et al* found that the electrical response using an SSHI interface circuit is similar to that using the standard interface under the strongly coupled condition [10]. The equivalent circuit and typical voltage, current, power waveforms of this technique are shown in figure 7. The circuit in figure 7(a) was further specified as 'parallel-SSHI' (P-SSHI) by Lefeuvre *et al* [8]. In SSHI, a parallel inductive switching shortcut is added to the SEH circuit for instant voltage inversion. It makes use of the natural response of the under-damped r–L_i–C_p circuit. Once the displacement x obtains its maxima or minima, e.g., 0 and π/ω instants in figure 7(b), the switch takes action to invert the

(a)

(b)
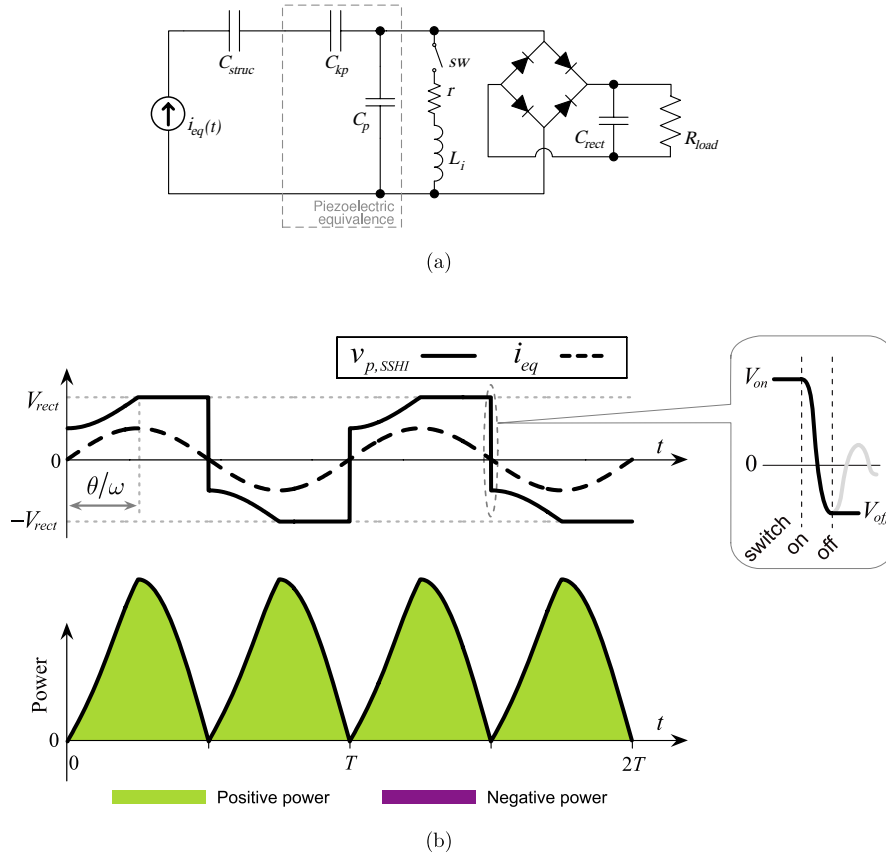
Figure 7. The SSHI interface circuit. (a) Circuit topology. (b) Typical waveforms.

voltage across the piezoelectric capacitance with the factor of

$$\gamma = \frac{V_{\text{off}}}{V_{\text{on}}} = -e^{-\pi/(2Q)} \tag{16}$$

where V_{on} and V_{off} are the voltages before and after the inversion, respectively; Q is the quality factor of the switching r–L_i–C_p circuit. One of the switching processes is zoomed in and shown in figure 7(b). These switching actions make the symbol of v_p change to that of i_{eq}. Therefore, the synchronized switching actions make v_p in phase with i_{eq}, which ensures that the power entering the electrical part is always positive. In addition, the magnitude of v_p is also increased by implementing the SSHI, which indicates that more energy is extracted from the source.

Given that the time constant of the electrical RLC circuit is much smaller than that of mechanical excitation, the voltage inversion takes place almost in an instant. Neglecting the time durations of the switching actions, the voltage across the piezoelectric element in SSHI is expressed by the following piecewise equation:

$$v_{\text{p,SSHI}}(t) =$$
$$\begin{cases} v_{\text{p,oc}}(t) - v_{\text{p,oc}}(0) - \gamma V_{\text{rect}}, & 0^+ \leqslant \omega t < \theta \\ V_{\text{rect}}, & \theta \leqslant \omega t \leqslant \pi^- \\ v_{\text{p,oc}}(t) - v_{\text{p,oc}}(\pi/\omega) + \gamma V_{\text{rect}}, & \pi^+ \leqslant \omega t < \pi + \theta \\ -V_{\text{rect}}, & \pi + \theta \leqslant \omega t \leqslant 2\pi^-. \end{cases} \tag{17}$$

Comparing (15) and (17), it can be concluded that SEH is a special case of SSHI, in which the voltage inversion factor $\gamma = 1$. Therefore, in the following part, we use one model to summarize the behaviors of these two PEH devices.

The blocked angle θ illustrated in figure 6(b) for SEH and figure 7(b) for SSHI is related to the non-dimensional rectified voltage with the following relation:

$$\cos\theta = 1 - (1 + \gamma)\tilde{V}_{\text{rect}} \tag{18}$$

where the non-dimensional rectified voltage is defined by

$$\tilde{V}_{\text{rect}} = \frac{V_{\text{rect}}}{V_{\text{OC}}}. \tag{19}$$

To quantify the characteristics of energy harvesting, energy dissipation and the effect on vibration damping, the charge–voltage diagram is employed to illustrate the energy conversion cycle. Since the short circuit stiffness of the device, which is represented by C in the equivalent circuit, is in series with the electrical part of the device, the charge flowing through both parts is the same, i.e., Q_{eq} given in (9). Figure 8(a) shows the charge–voltage locus of the equivalent capacitance C. Since the charge and voltage are in phase for pure capacitance, the locus overlaps on the straight line. The vibratory energy corresponds to the area that is first covered by the $v\,\mathrm{d}Q > 0$ (positive power) segments in the locus, and then covered by the $v\,\mathrm{d}Q < 0$ segments (negative power) in a half
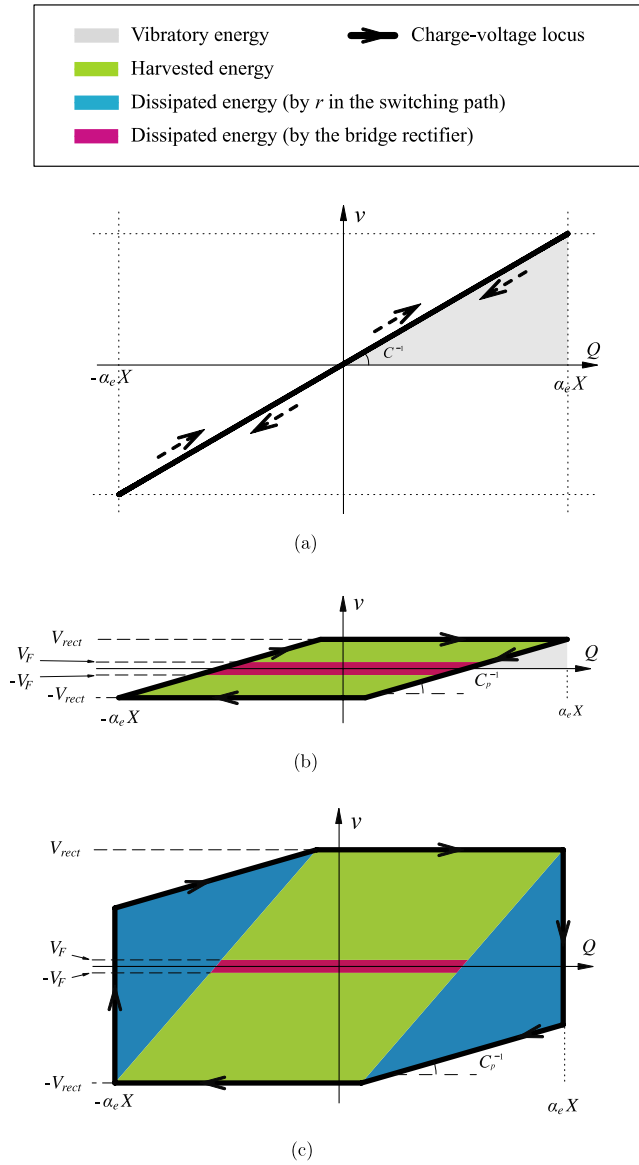
Figure 8. Charge–voltage diagrams. (a) Mechanical part.
(b) Electrical part ($\gamma = 1$, $\tilde{V}_{\text{rect}} = 0.45$, $\theta = 1.47$). (c) Electrical part
($\gamma = -0.5$, $\tilde{V}_{\text{rect}} = 1.8$, $\theta = 1.47$).

cycle. Therefore, the vibratory energy in the mechanical part corresponds to the gray area in figure 8(a).

Figures 8(b) and (c) show the charge–voltage locus of the electrical part under two conditions, respectively[3]. The first condition ($\gamma = 1$) corresponds to the SEH case. In figure 8(b), the gray area represents the vibratory energy in the electrical part. The area enclosed by the locus corresponds to the energy that is extracted from the system. Some part of the extracted energy is harvested (in green), while some part of it is dissipated by the bridge rectifier (in red), because of the non-zero forward voltage drop. The second condition ($\gamma = -0.5$) corresponds to the SSHI case. There is no gray area in figure 8(c), because no energy returns from the electrical

[3] In the printed version the lightest, lighter, darker and darkest gray correspond to the colors gray, green, blue and red in the electronic version, respectively.

to the mechanical part in SSHI, i.e., no vibratory energy in the electrical part. The enclosed area can be subdivided into three portions: harvested energy (in green), energy dissipated by the resistance r in the switching path (in blue), and energy dissipated by the bridge rectifier (in red). Without energy returning from the electrical to the mechanical part in the SSHI case, the energy flow chart does not have branch **J**.

From the energy conversion cycle shown in figure 8, and based on the geometric relations among the area in different colors, we can calculate the four branches of energy flow, i.e., vibratory energy E_{max}, harvested energy E_{h}, dissipated energy E_{d}, and extracted energy ΔE. The vibratory energy is composed of the two portions in SEH, mechanical and electrical, while it only has the mechanical portion in SSHI:

$$E_{\text{max}} = \frac{1}{2}C_{\text{p}}V_{\text{OC}}^2 * \begin{cases} \dfrac{1 - k_{\text{d}}^2}{k_{\text{d}}^2}, & -1 < \gamma \leqslant 0 \\[2ex] \left(\dfrac{1 - k_{\text{d}}^2}{k_{\text{d}}^2} + \gamma^2 \tilde{V}_{\text{rect}}^2 \right), & 0 < \gamma \leqslant 1. \end{cases}$$
$$(20)$$

The amount of energy harvested in one cycle is

$$E_{\text{h}} = 2C_{\text{p}}V_{\text{OC}}^2(\tilde{V}_{\text{rect}} - \tilde{V}_{\text{F}})[2 - \tilde{V}_{\text{rect}}(1 + \gamma)] \qquad (21)$$

where $\tilde{V}_{\text{F}}$ is the non-dimensional voltage drop of the diode, which is defined as

$$\tilde{V}_{\text{F}} = \frac{V_{\text{F}}}{V_{\text{OC}}}. \qquad (22)$$

To ensure that the harvested energy is greater than or equal to zero, the range of $\tilde{V}_{\text{rect}}$ should be

$$\tilde{V}_{\text{F}} \leqslant \tilde{V}_{\text{rect}} \leqslant \frac{2}{1 + \gamma}. \qquad (23)$$

The maximum E_{h} is obtained at the optimized rectified voltage

$$\tilde{V}_{\text{rect,opt}} = \frac{1}{1 + \gamma} + \frac{\tilde{V}_{\text{F}}}{2}. \qquad (24)$$

This $\tilde{V}_{\text{rect,opt}}$ is in the middle of the harvestable range given in (23). The amount of energy dissipated in one cycle is
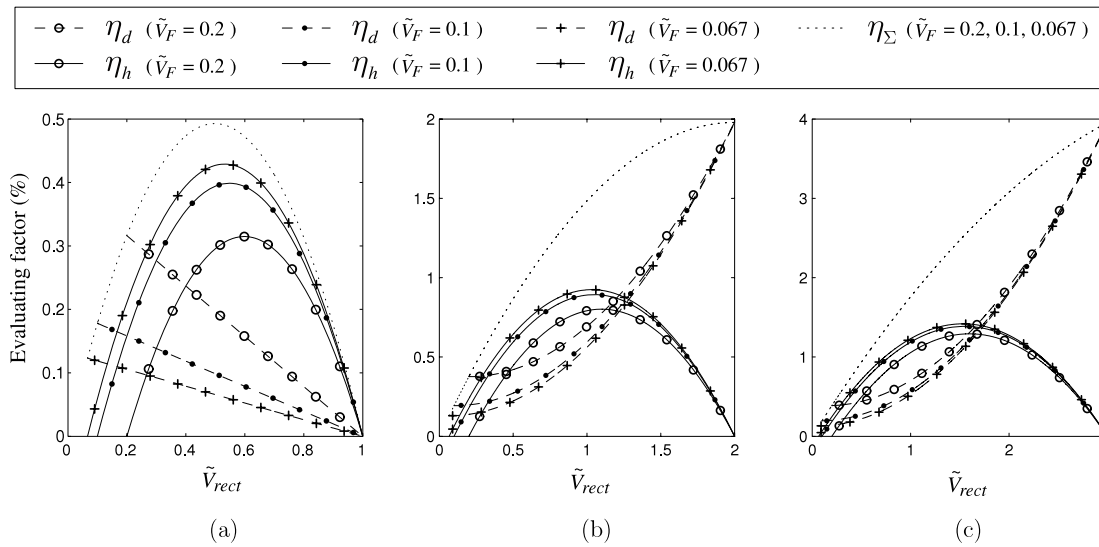
$$E_{\text{d}} = C_{\text{p}}V_{\text{OC}}^2\{\tilde{V}_{\text{rect}}^2(1 - \gamma^2) + 2\tilde{V}_{\text{F}}[2 - \tilde{V}_{\text{rect}}(1 + \gamma)]\}. \quad (25)$$

The first item in (25) represents the energy dissipation in r during the switch action; the second item results from the voltage drop across the bridge rectifier. The total extracted energy is the sum of both the harvested and dissipated energies:
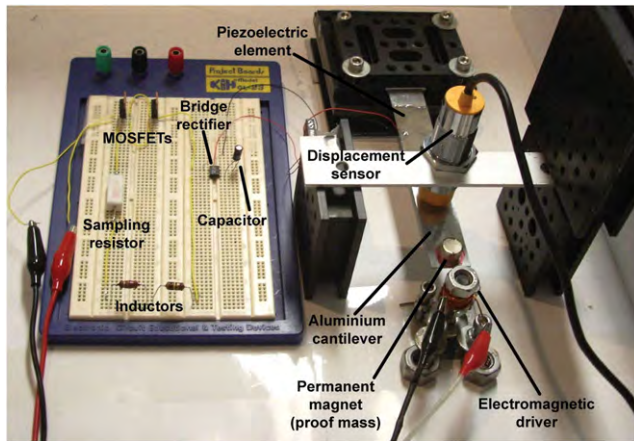
$$\Delta E = E_{\text{h}} + E_{\text{d}} = C_{\text{p}}V_{\text{OC}}^2[4\tilde{V}_{\text{rect}} - \tilde{V}_{\text{rect}}^2(1 + \gamma)^2]. \quad (26)$$

Substituting (20), (21), (25), and (26) for E_{max}, E_{h}, E_{d}, and ΔE into (12)–(14), the harvesting factor η_{h}, dissipation factor η_{d} and loss factor η_{Σ} can be obtained, respectively.

Figure 9 shows the three evaluating factors as functions of $\tilde{V}_{\text{rect}}$ under three γ and three $\tilde{V}_{\text{F}}$. It can be observed that smaller γ enables the three factors to attain larger values; yet, the extent of dissipation factor increases much faster than the harvesting factor. The range of $\tilde{V}_{\text{rect}}$ also gets larger with smaller γ. On the other hand, under the same γ, $\tilde{V}_{\text{F}}$ has no relation with

7

Figure 9. Evaluating factors under different γ and $\tilde{V}_F$. (a) $\gamma = 1$ (SEH). (b) $\gamma = 0$. (c) $\gamma = -0.33$.

Figure 10. Experimental setup for PEH with the SSHI technique.

Table 1. Models or values of different components in the SSHI circuit.

Component	Value or model
C_p	34.76 nF
sw	MOSFET (IRF530N)
L_i	121.8 mH
Bridge rectifier	DB104 ($V_F = 1.0$ V)
C_{rect}	9.708 μF
r_{sample}	10.2 Ω

three evaluating factors that are defined in (12)–(14) are better measured independently. In their study on the damping effect of the SEH device, Lesieutre *et al* [16] measured the performances on harvesting and damping with two different methods. In this section, three experiments based on different principles are carried out on an SSHI device to estimate the loss factor, harvesting factor and dissipation factor.

Figure 10 shows the mechanical structure and the harvesting circuit in the experimental setup. The main mechanical structure is an aluminum cantilever whose fixed end is fixed on the vibration-free table and the free end is driven by an electromagnetic driver. A piezoceramic patch of 49 mm × 24 mm × 0.508 mm (T120-A4E-602, Piezo System, Inc.) is bonded near the fixed end where the largest strain happens along the cantilever. A permanent magnet is attached at the free end of the cantilever, so as to achieve the coupling with the electromagnetic driver; and it also acts as a proof mass to lower the vibration frequency and increase the displacement of the free end. The displacement of the cantilever is sensed by an inductive displacement sensor (JCW-24SR, CNHF Co.). Applying a 25 Hz harmonic excitation, which corresponds to a 1.34 V peak–peak value output from the displacement sensor, to this structure, a 16.6 V peak–peak value sinusoidal voltage can be observed across the piezoelectric element.

In order to perform synchronized switching actions, the displacement sensor output is connected to an A/D channel of the PC based controller board (dSPACE DS1104). The digital

the loss factor; it influences the distribution of the extracted energy between the harvesting and dissipation portions, as well as the harvestable range. The larger the $\tilde{V}_F$, the more energy is dissipated, while the less is harvested. The harvestable range becomes smaller with a larger $\tilde{V}_F$. In addition, the influence of $\tilde{V}_F$ on the differences in both the harvesting and dissipation factors gets smaller with smaller γ.

5. Experiments

Experiments are carried out, in order to verify the theoretical analysis on energy flow in PEH with an SSHI interface circuit. Previous experimental results on PEH devices were mostly focused on the harvested energy [7–9, 29]. Guyomar *et al* [18] considered the extracted energy for comparison to the harvested energy; their results on extracted energy are indirectly obtained from the harvested energy, rather than measured. To experimentally study the performances on energy harvesting, dissipation, and structural damping, the

Figure 11. Frequency response functions under different electrical conditions.

processor performs peak detection and generates a switch driving signal accordingly to control the switch in the SSHI circuit. The harvesting circuit is shown on the left-hand side of figure 10. Table 1 gives the models or values of different components in the circuit.

The coupling coefficient of the main structure, k_d^2, is fixed after installation; meanwhile the Q factor of the switching shunt is fixed when all components are connected, i.e., γ is fixed. According to (20), (21), (25), and (26), the three evaluating factors corresponding to structural damping, energy harvesting and energy dissipation are all functions of $\tilde{V}_{rect}$. The functional relations can be investigated experimentally as follows.

5.1. Loss factor on structural damping

As the loss factor is related to the system bandwidth that can be obtained from the frequency response function (FRF)[4], the loss factors under different electrical conditions, i.e., short circuit, open circuit and seven values of $\tilde{V}_{rect}$ (from 5/12 to 35/12 with a step of 5/12), can be estimated with this method. For each condition, the peak–peak values of the displacement sensor outputs at 18 frequencies (24.0–25.7 Hz with a step of 0.1 Hz) are recorded. To obtain the displacement peak–peak values under different $\tilde{V}_{rect}$, V_{rect} should be adjusted according to the changing V_{OC}, which cannot be directly measured when the SSHI is operating. However, since V_{OC} is proportional to X, the maximum displacement of the structure, it can still be indirectly obtained under SSHI operation. To adjust V_{rect}, the constant voltage output of a power supply (IPS 2303D, ISO-TECH) is connected to the capacitor C_{rect}. Nine FRF curves are obtained by fitting the corresponding data under each condition[5]. Figure 11 shows the measured data and fitted

curves. For each curve, the resonant frequency f_0 and the -3 dB bandwidth Δf can be calculated. Therefore, the loss factor under the corresponding condition is $\Delta f / f_0$. Since the loss factors include both inherent mechanical damping and the damping contributed by the SSHI, subtracting the loss factors under different $\tilde{V}_{rect}$ from that under short circuit condition yields the net contribution of the SSHI [16].

5.2. Harvesting factor on energy harvesting

The harvesting factor is estimated based on (12). With the record of a complete charging process, E_h can be obtained from the voltage history across C_{rect}; meanwhile, E_{max} can be obtained from the displacement history. The voltage and displacement histories are separated into a number of appropriate intervals. Within an interval, V_{rect} is regarded as the sum of V_F and the mean voltage across C_{rect}. The energy harvested during this interval can be calculated with respect to the voltage increase across C_{rect}. As illustrated in figure 12, the mean voltage across the storage capacitor within an interval in the charging history is assumed to be constant during charging. The harvested power under this V_{rect} can be obtained, because the energy input of the capacitor within such interval can be estimated according to the voltage change. However, there is a problem that the estimating interval should be chosen carefully. If it is too long, the constant voltage assumption would be invalid; on the contrary, if it is too short, the voltage across the capacitor can hardly change. We overcome this problem with an 'adaptive interval algorithm'. Generally, a shorter interval for lower V_{rect} and a longer one for higher V_{rect}, since the voltage changes more sharply at low V_{rect}.

E_{max} in SSHI only includes mechanical vibratory energy, so it is related to the maximum displacement. Since 1.34 V peak–peak value output from the displacement sensor corresponds to 16.6 V peak–peak value sinusoidal voltage across the open circuit piezoelectric element, the mechanical vibratory energy associated with 1.34 V peak–peak value displacement output can be estimated with the device coupling coefficient, which can be calculated with the resonant frequencies under open circuit and short circuit conditions with the following relation:

$$k_d^2 = \frac{f_{OC}^2 - f_{SC}^2}{f_{OC}^2}. \tag{27}$$
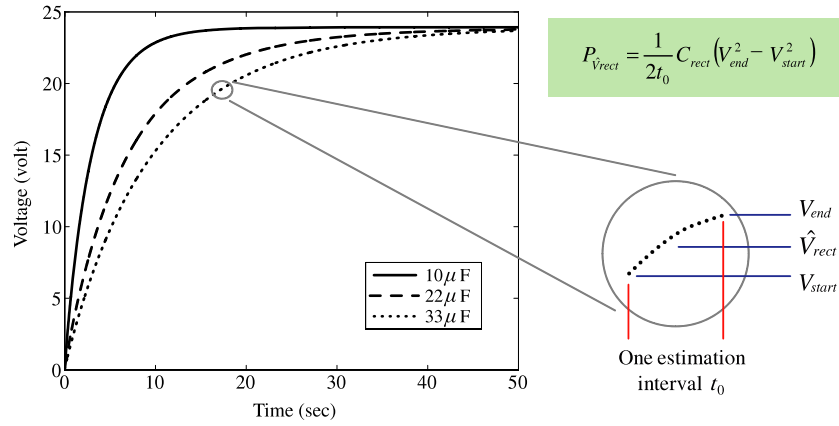
From figure 11, the open circuit natural frequency $f_{OC} = 24.69$ Hz, the short circuit natural frequency $f_{SC} = 24.50$ Hz, therefore $k_d^2 = 0.0153$. This means, in the open circuit, when the voltage across C_p is at maximum, i.e., 8.3 V, the ratio between mechanical energy and electrical energy is $(1 - k_d^2)/k_d^2$. Knowing the E_{max} associated with 1.34 V peak–peak value displacement output, the E_{max} associated with other displacement values can be obtained.

5.3. Dissipation factor on energy dissipation

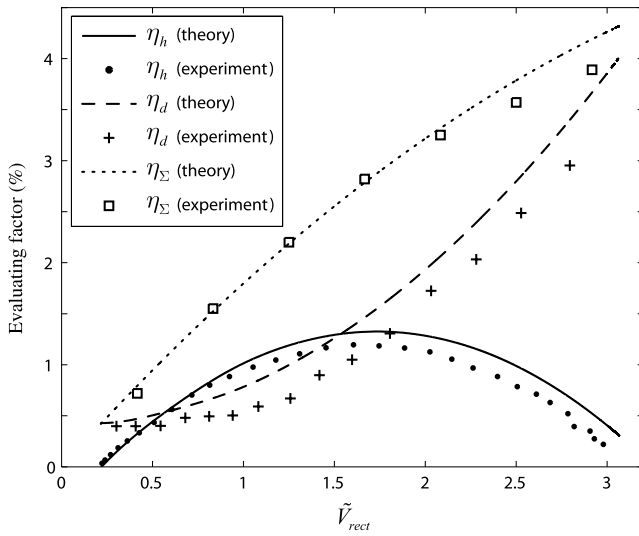The dissipation factor is estimated based on (13). From the voltage across C_p, the voltage inversion factor γ is obtained to be -0.384. So the Q factor of the switching shunt is about

$$P_{\dot{V}rect} = \frac{1}{2t_0} C_{rect} \left(V_{end}^2 - V_{start}^2 \right)$$

Figure 12. Estimation of harvested power from the history of v_p.

Figure 13. Theoretical and experimental results on three evaluating factors in PEH with an SSHI interface.

1.64, the total equivalent series resistance r is 1.14 kΩ. Since a 10 Ω sampling resistor r_{sample} is connected in series to the shunt, recording the root mean square (RMS) voltage across r_{sample} under different V_{rect} with an oscilloscope (TDS 220, Tektronix), the energy consumed by r in one cycle can be estimated. As for the energy dissipated by the bridge rectifier in one cycle, i.e., the second item in (25), it is proportional to E_h under certain V_{rect}; therefore it can be calculated simultaneously with the estimation of E_h. Combining these two dissipations, E_d is readily obtained.

5.4. Comparison

Three experiments are performed in order to show the functional relations of η_h, η_d and η_Σ with $\tilde{V}_{rect}$. Besides, since k_d^2 and γ are experimentally obtained as 0.0153 and -0.384, respectively, the three evaluating factors are also readily theoretically obtained with (12)–(14). Both results are simultaneously shown in figure 13. It demonstrates that both

experimental results and theoretical analyses agree with each other very well.

6. Conclusion

A detailed analysis on the energy flow in piezoelectric energy harvesting (PEH) systems was presented in this paper. The concept of energy flow was clarified and illustrated with the energy flow chart. Previously, absolute harvested power was usually considered to evaluate different PEH devices. This is an application-oriented evaluation. But looking into the PEH devices, for an overall evaluation, we suggest that three evaluating factors (harvesting factor, dissipation factor, and loss factor) are likewise important, since they are helpful to quantify each branch of the energy flow within different PEH devices. For the PEH devices with standard energy harvesting (SEH) and synchronized switch harvesting on inductor (SSHI) interface circuits, quantitative analyses revealed the coexistent relation of energy harvesting and energy dissipation, as well as their combined effect on structural damping. In SSHI, it was even reported that this technique can significantly increase the harvesting efficiency, it could also bring out the increase on energy dissipation. In particular, for larger $\tilde{V}_{rect}$, the dissipation factor can be larger than the harvesting factor, i.e., more energy is dissipated rather than harvested in one cycle.

Generally speaking, in every PEH device, energy dissipation inevitably exists. The coexistent relation between energy harvesting and dissipation is subtle. For the purpose of making good recycling of the ambient vibration energy, the understanding of their relation and their total effect on the vibrating structure is crucial towards future development of PEH devices. In addition, the energy flow based framework proposed in this paper can also be applied to the study of other mechanical to electrical energy conversion devices.

Acknowledgment

References

[1] Liao W H, Wang D H and Huang S L 2001 Wireless monitoring of cable tension of cable-stayed bridges using PVDF piezoelectric films *J. Intell. Mater. Syst. Struct.* **12** 331–9

[2] Anton S R and Sodano H A 2007 A review of power harvesting using piezoelectric materials (2003–2006) *Smart Mater. Struct.* **16** R1–21

[3] Sodano H A, Park G and Inman D J 2004 Estimation of electric charge output for piezoelectric energy harvesting *Strain* **40** 49–58

[4] Erturk A and Inman D 2008 On mechanical modeling of cantilevered piezoelectric vibration energy harvesters *J. Intell. Mater. Syst. Struct.* **19** 1311–25

[5] Zhu M, Worthington E and Njuguna J 2009 Analyses of power output of piezoelectric energy-harvesting devices directly connected to a load resistor using a coupled piezoelectric-circuit finite element method *IEEE Trans. Ultrason. Ferroelectr. Freq. Control* **56** 1309–17

[6] Stanton S C, McGehee C C and Mann B P 2010 Nonlinear dynamics for broadband energy harvesting: investigation of a bistable piezoelectric inertial generator *Physica* D **239** 640–53

[7] Ottman G K, Hofmann H F, Bhatt A C and Lesieutre G A 2002 Adaptive piezoelectric energy harvesting circuit for wireless remote power supply *IEEE Trans. Power Electron.* **17** 669–76

[8] Lefeuvre E, Badel A, Richard C, Petit L and Guyomar D 2006 A comparison between several vibration-powered piezoelectric generators for standalone systems *Sensors Actuators* A **126** 405–16

[9] Qiu J, Jiang H, Ji H and Zhu K 2009 Comparison between four piezoelectric energy harvesting circuits *Front. Mech. Eng. China* **4** 153–9

[10] Shu Y C, Lien I C and Wu W J 2007 An improved analysis of the SSHI interface in piezoelectric energy harvesting *Smart Mater. Struct.* **16** 2253–64

[11] Liu Y, Tian G, Wang Y, Lin J, Zhang Q and Hofmann H F 2009 Active piezoelectric energy harvesting: general principle and experimental demonstration *J. Intell. Mater. Syst. Struct.* **20** 575–85

[12] Liu W Q, Feng Z H, He J and Liu R B 2007 Maximum mechanical energy harvesting strategy for a piezoelement *Smart Mater. Struct.* **16** 2130–6

[13] Scruggs J T 2010 On the causal power generation limit for a vibratory energy harvester in broadband stochastic response *J. Intell. Mater. Syst. Struct.* doi:10.1177/1045389X10361794

[14] Lu F, Lee H P and Lim S P 2004 Modeling and analysis of micro piezoelectric power generators for micro-electromechanical-systems applications *Smart Mater. Struct.* **13** 57–63

[15] Kim H, Priya S, Stephanou H and Uchino K 2007 Consideration of impedance matching techniques for efficient piezoelectric energy harvesting *IEEE Trans. Ultrason. Ferroelectr. Freq. Control* **54** 1851–9

[16] Lesieutre G A, Ottman G K and Hofmann H F 2004 Damping as a result of piezoelectric energy harvesting *J. Sound Vib.* **269** 991–1001

[17] Liang J R and Liao W H 2009 Piezoelectric energy harvesting and dissipation on structural damping *J. Intell. Mater. Syst. Struct.* **20** 515–27

[18] Guyomar D, Sebald G, Pruvost S, Lallart M, Khodayari A and Richard C 2009 Energy harvesting from ambient vibrations and heat *J. Intell. Mater. Syst. Struct.* **20** 609–24

[19] Beeby S P, Tudor M J and White N M 2006 Energy harvesting vibration sources for microsystems applications *Meas. Sci. Technol.* **17** R175–95

[20] Priya S and Inman D J 2009 *Energy Harvesting Technologies* (New York: Springer)

[21] Elvin N G and Elvin A A 2009 A coupled finite element–circuit simulation model for analyzing piezoelectric energy generators *J. Intell. Mater. Syst. Struct.* **20** 587–95

[22] Yang Z and Yang J 2009 Connected vibrating piezoelectric bimorph beams as a wide-band piezoelectric power harvester *J. Intell. Mater. Syst. Struct.* **20** 569–74

[23] Guan M J and Liao W H 2009 On the equivalent circuit models of piezoelectric ceramics *Ferroelectrics* **386** 77–87

[24] Guan M J and Liao W H 2007 On the efficiencies of piezoelectric energy harvesting circuits towards storage device voltages *Smart Mater. Struct.* **16** 498–505

[25] Wu W J, Wickenheiser A M, Reissman T and Garcia E 2009 Modeling and experimental verification of synchronized discharging techniques for boosting power harvesting from piezoelectric transducers *Smart Mater. Struct.* **18** 055012

[26] Shu Y C and Lien I C 2006 Analysis of power output for piezoelectric energy harvesting systems *Smart Mater. Struct.* **15** 1499–512

[27] Mitcheson P D, Yeatman E M, Rao G K, Holmes A S and Green T C 2008 Energy harvesting from human and machine motion for wireless electronic devices *Proc. IEEE* **96** 1457–86

[28] Paradiso J A and Starner T 2005 Energy scavenging for mobile and wireless electronics *IEEE Pervasive Comput.* **4** 18–27

[29] Guyomar D, Badel A, Lefeuvre E and Richard C 2005 Toward energy harvesting using active materials and conversion improvement by nonlinear processing *IEEE Trans. Ultrason. Ferroelectr. Freq. Control* **52** 584–95

[30] Clark W W 2000 Vibration control with state-switched piezoelectric materials *J. Intell. Mater. Syst. Struct.* **11** 263–71

[31] Ji H, Qiu J, Zhu K and Badel A 2010 Two-mode vibration control of a beam using nonlinear synchronized switching damping based on the maximization of converted energy *J. Sound Vib.* **329** 2751–67

[32] Hu Y, Xue H, Hu T and Hu H 2008 Nonlinear interface between the piezoelectric harvesting structure and the modulating circuit of an energy harvester with a real storage battery *IEEE Trans. Ultrason. Ferroelectr. Freq. Control* **55** 148–60